In vivo hyperspectral CARS and FWM microscopy of carotenoid accumulation in *H. Pluvialis.*

Aaron D. Slepkov,*[a] Aaron M. Barlow,[b,c] Andrew Ridsdale,[b] Patrick J. McGinn,[d] Albert Stolow [b,c]
[a]Department of Physics & Astronomy, Trent University, Peterborough ON, K9J7B8, Canada;
[b]SDT, Emerging Technologies Division, National Research Council of Canada, 100 Sussex Dr., Ottawa ON, K1A 0R6, Canada;
[c]Department of Physics, University of Ottawa, Ottawa ON, K1N 6N5, Canada;
[d]Carbon Conversion Flagship Program, National Research Council of Canada, 1411 Oxford St., Halifax, NS, B3H 3Z1, Canada

ABSTRACT

Coherent anti-Stokes Raman scattering (CARS) and four-wave-mixing (FWM) microscopy are a related pair of powerful nonlinear optical characterization tools. These techniques often yield strong signals from concentrated samples, but because of their quadratic dependence on concentration, they are not typically employed for imaging or identifying dilute cellular constituents. We report here that, depending on the excitation wavelengths employed, both CARS and degenerate-FWM signals from carotenoid accumulations in alga cysts can be exceptionally large, allowing for low-power imaging of astaxanthin (AXN) deposits in *Haematococcus pluvialis* microalga. By use of a broadband laser pulse scheme for CARS and FWM, we are able to simultaneously collect strong intrinsic two-photon-excitation fluorescence signals from cellular chlorophyll *in vivo*. We show that CARS signals from astaxanthin (AXN) samples *in vitro* strictly follow the expected quadratic dependence on concentration, and we demonstrate the collection of well-resolved CARS spectra in the fingerprint region with sensitivity below 2mM. We suggest that multimodal nonlinear optical microscopy is sufficiently sensitive to AXN and chlorophyll concentrations that it will allow for non-invasive monitoring of carotenogenesis in live *H. pluvialis* microalgae.

Keywords: Coherent anti-Stokes Raman scattering, four-wave-mixing, nonlinear optical microscopy, carotenogenesis, astaxanthin, chlorophyll, *Haematococcus pluvialis*.

1. INTRODUCTION

Astaxanthin (AXN) is a ketocarotenoid, biochemically related to β-carotene, which is used as a powerful antioxidant and natural colourant in dyes, cosmetics, naturaceuticals, and food additives, and has current world-wide sales exceeding a hundred million dollars.[1-4] Traditionally, the majority of commercial and scientific grade AXN has been produced synthetically, but recently natural sources such as krill, shrimp, yeast and microalgae are becoming economically important. One notable source of AXN is *Haematococcus pluvialis, a* widespread unicellular green microalgae found in freshwater ponds and rainwater pools.[5] Typically, *H. pluvialis* are small and motile, with pigmented cellular contents dominated by chlorophyll. Upon exposure to unfavorable conditions, however, the algae synthesize large amounts of AXN and swell into large cysts, at which point AXN comprises a significant proportion of the cells' dry weight.[6-7] Most cellular carotenoids are typically plastid-associated, but it is becoming increasingly clear that, in *H. pluvialis*, AXN accumulates within lipid drops, often in the center of the cyst.[8-9] The spatial and biochemical relationship between chloroplasts and carotenogenesis, however is a subject of ongoing research.[7,10] Both for biological and technological reasons, there is strong interest in understanding and quantifying carotenogenesis in *H. pluvialis*.

*contact: aaronslepkov@trentu.ca

Multimodal Biomedical Imaging IX, edited by Fred S. Azar, Xavier Intes, Proc. of SPIE
Vol. 8937, 893709 · © 2014 SPIE · CCC code: 1605-7422/14/$18 · doi: 10.1117/12.2038229

The very large resonance-Raman cross-sections in carotenoids have engendered several studies using confocal Raman microscopy to study the distribution of carotenoids within microalgae.[11,12] Such an approach has also been used to map the synthesis of β-carotene to AXN throughout the algal life cycle.[13] Other techniques such as transmission electron microscopy have mapped the intracellular morphologies at key points in the algal life cycle and demonstrated that the degradation of the chloroplast is concurrent with AXN production.[10] Nonetheless, a method for rapid label-free imaging, correlating lipid with AXN distributions, and assaying of cellular carotenoid contents in live cells has not yet been established.

In this work, we demonstrate the effectiveness of nonlinear microscopy as a powerful label-free imaging modality for the rapid study of AXN *in vivo*.[14] We employ coherent anti-Stokes Raman scattering (CARS) microscopy, a vibrationally-resonant four-wave-mixing technique to directly image AXN with spectral contrast in the Raman fingerprint region. Using broadband ultrafast laser pulses we are able to simultaneously collect CARS and other nonlinear optical modalities such as two-photon-excitation-fluorescence (TPEF),[15] which can be used for concurrent label-free mapping of intracellular chlorophyll content.[16,17] Alternately, simply by tuning the excitation laser to a different wavelength range, we show that the same microscope system and procedure yields non-vibrationally-resonant four-wave-mixing (FWM) signals from AXN which are sufficiently strong to enable live cell imaging. Typically, the nondegenerate-FWM signal acts as an unwanted nonresonant background which interferes with the CARS signal, significantly reshaping and complicating its spectrum.[18,19] In recent years, however, degenerate-FWM has itself attracted interest as a contrast mechanism in microscopy.[20-22] FWM microscopy is most commonly applied to inorganic materials, where signals can be enhanced by exploiting electronic or plasmonic resonance enhancement.[20] There are few examples of this technique being applied to biological systems.[23] We show that, depending on the pump wavelength, either CARS or degenerate-FWM can be used for high-contrast, background-free imaging of cellular AXN. Both of these nonlinear optical techniques provide several key advantages: high-sensitivity; chemical specificity; rapid, three-dimensional scanning capability; and non-destructive live-cell imaging. However, unlike FWM, CARS can also provide detailed vibrational spectral information. Like Raman scattering, CARS is label-free and chemically specific; however, because of its stimulated nature, the CARS signal intensities can be orders of magnitude stronger than those from traditional Raman scattering.[24] The focal-excitation scheme of the nonlinear optical CARS process allows for fully three-dimensional images to be produced, where each pixel contains a vibrational spectrum of the sample—so called hyperspectral imaging.[19,25-27] We show that CARS signals from dilute AXN samples are dominated by the vibrationally-resonant signal and, therefore, the spectral characteristics remain qualitatively unchanged from that of spontaneous Raman techniques, but with signals orders of magnitude larger, allowing for orders of magnitude faster hyperspectral imaging.

2. EXPERIMENTAL

1.1 Optical layout for CARS and FWM microscopy

For hyperspectral CARS imaging in the fingerprint region, we modified an established multimodal CARS microscopy system, based on a single Ti:sapphire source and supercontinuum generation in a microstructured fibre, as described elsewhere.[27,28] A diagram of the set-up is shown in Figure 1. Briefly, 60 fs pulses at a repetition rate of 80 MHz are generated by a Ti:sapphire oscillator (Mira900, Coherent) and compressed by a prism-pair. A portion of this transform-limited pump/probe beam is then directed to a PCF module (FemtoWhite-CARS, NKT Photonics) for supercontinuum generation. The output of the PCF (Stokes) is filtered to remove <950 nm light, and recombined with the remaining pump/probe light which has passed through a variable delay line. Two fixed blocks of high-dispersion SF-6 glass are used to match the linear chirp-rates of the Stokes and pump/probe beams, with a 5-cm-long block inserted in the Stokes arm between the PCF and beam combiner and a 10-cm-long block inserted in the combined arm. By matching the chirp rates of these overlapping pulses, one controls their instantaneous interaction bandwidth and optimizes the spectral resolution for a given amount of dispersion in the pump pulse. This is known as spectral focusing.[28,29] Furthermore, by scanning the delay time between the pump and Stokes pulses, the CARS resonant frequency may be easily and rapidly tuned. Typically, the degenerate FWM process occurs concurrently and interferes with the vibrationally-resonant CARS process. This FWM signal is often referred to as the nonresonant background (NRB) signal in CARS spectroscopy. In this experiment we find that, depending on the excitation wavelength scheme we employ, the FWM signal itself can provide chemically-selective contrast for carotenoids. Experimentally, CARS and FWM imaging of carotenoids in *H. pluvialis* differ only in the pump wavelength utilized, and thus do not require any

modification of the experimental setup beyond the pump laser central frequency. For CARS hyperspectroscopy we use pump wavelengths between 880 nm and 920 nm; for FWM imaging we use pump wavelengths between 780 nm and 850 nm. In both cases, the broadband "Stokes" beam spans the 950 nm – 1200 nm range. For the data presented here, we used a pump wavelength of 915 nm for CARS and 830 nm for FWM. The excitation schemes for FWM and CARS are depicted, to scale, and overlaid on an energy level diagram for AXN in Figure 2.

A FV300 Fluoview Olympus microscope was modified to allow for non-descanned CARS/FWM signal collection in the forward-direction via a multimodal optical fiber coupled to an off-board red-enhanced PMT detector, as described elsewhere.[30] A 40× 1.15 NA water-immersion lens with cover-slip correction was used for imaging and spectroscopy (Olympus UAPON 40XW340). The TPEF signal was simultaneously recorded via on-board descanned epi-detection. For CARS/FWM imaging of AXN and alga cysts, we used pump powers of 0.5-3.0 mW, and broadband Stokes powers of 1.5-3.0 mW, at the sample location. These powers are considerably lower than we typically employ for CARS imaging of other biological systems.[30-33] By contrast, for DMSO characterization by CARS we used ~30 mW of pump power, and 3.0 mW of Stokes power, at the sample location.

1.2 Sample preparation

Live samples of *H. pluvialis*, suspended in aqueous media, were obtained from labs of the National Research Council of Canada's Institute for Marine Biosciences. In preparation for studying under the microscope, the samples were briefly shaken and aspirated between a microscope slide and coverslip. Periodically, we found it necessary to inject additional water into the sample to ensure that the algae remained hydrated throughout the experiment. Inspection of the samples suggested that the vast majority of cells were in the cyst form, as no motile flagellated *H. pluvialis* cells were observed. Because *in vivo* AXN is acylated, *in vitro* comparisons should be conducted with similarly acylated carotenoids. AstaReal 10L® is a commercially-available concentrated AXN product derived from *H. pluvialis* produced by AstaReal, a company of Fuji Chemical Industry Group. It is nominally 10% AXN by weight (as free-form AXN) dispersed in a viscous tar-like matrix. Reference samples of AXN were made by dilution of AstaReal10L in food-grade

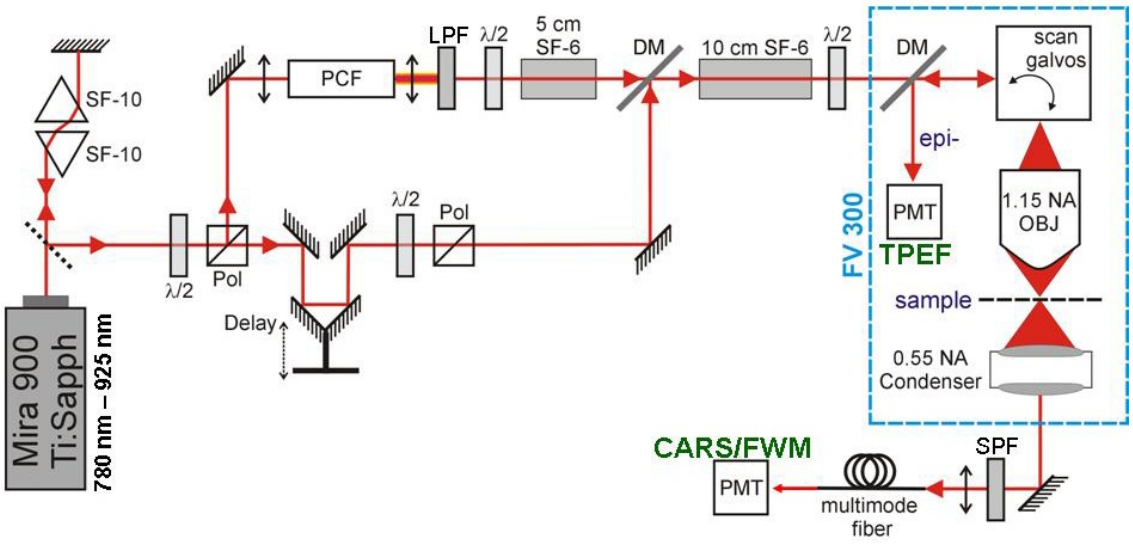

Figure 1. Optical layout for single-source multimodal CARS and degenerate FWM microscopy. 60 fs pulses from a Ti:sapphire oscillator are sent through a prism compressor before being split by a variable beam splitter. One arm is sent through a photonic crystal fiber (PCF) where it generates broadband supercontinuum "Stokes" pulses. This beam then passes to a long-pass (λ>900 nm) filter (LPF) and a 5-cm-long block of SF-6 before being recombined on a dichroic mirror (DM). The other beam is sent through a time delay arm and a variable attenuator. The two beams are recombined and then passed through an additional 10-cm of SF-6 glass before being routed into an Olympus FV300 microscope. The forward-propagating CARS/FWM signals are separated from the excitation pulses with a short-pass (λ<730 nm) filter (SPF), collected in a non-descanned geometry through a multimode fiber and are routed to off-board detectors. Pol: polarizer; λ/2: half-wave plate; OBJ: objective; PMT; photomultiplier tubes. For CARS imaging of AXN, the laser is tuned to wavelengths between 880 nm and 920 nm (nominally 915 nm), and for degenerate FWM imaging of AXN the laser is tuned to wavelengths between 780 nm and 850 nm (nominally 830 nm). The PCF output spectrum is not strongly dependent on input laser wavelength between 780 nm and 920 nm.

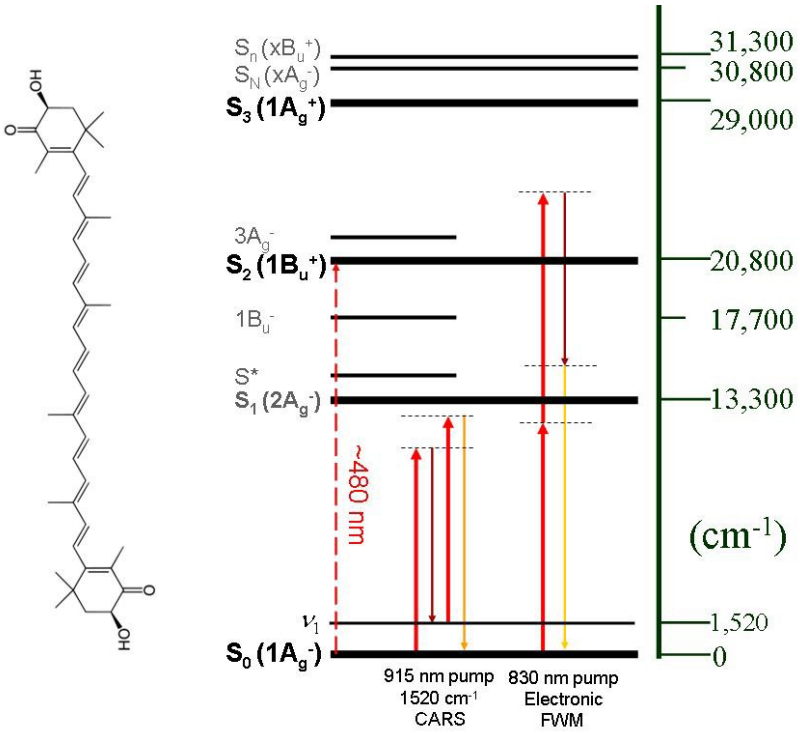

Figure 2. Known energy levels in AXN overlaid with experimental excitation scheme used for CARS and FWM. The lowest electronic transition, $S_0 \rightarrow S_1$ is one-photon forbidden. In the left scheme, for CARS signals from the ν_1 vibrational mode in AXN, pump and probe wavelengths of 915 nm (red arrows) are 1520 cm^{-1} higher in frequency than the Stokes wavelength of 1062 nm (smallest downwards arrow, brown), and the collected anti-Stokes signal is at 803 nm (largest downward arrow; yellow). None of these wavelengths appears to be resonant with a known dipole transition.[42] In the scheme on the right, for strong degenerate FWM signals in AXN, the pump wavelength is 830 nm (red arrows), and the signal is detected nominally at 650 nm (large yellow downwards arrow). Note that in this case the process does not appear to be resonant with any one- or two-photon allowed transitions. The chemical structure of astaxanthin is shown on the left.

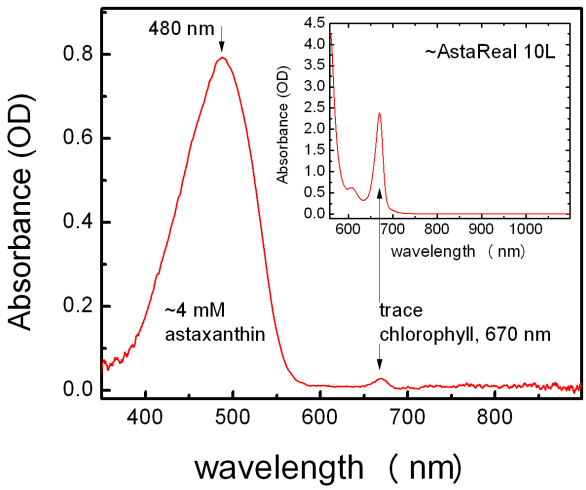

Figure 3. Absorption spectrum of naturally-derived acylated AXN *in vitro*. Main: AstaReal 10L® reference material diluted to approximately 4 mM free AXN in canola oil. Inset: Full concentration AstaReal 10L®. Trace amounts of cellular chlorophyll are found to be present by a characteristic absorption peak at 670 nm. The absorption spectrum is dominated by the main S0→S2 transition in AXN at 480 nm, and no identifiable absorption is measured at any wavelengths above 670 nm, precluding simple dipole-mediated resonance enhancement effects of the CARS process.

canola oil. AXN concentrations were then further confirmed by UV-Vis absorption spectra, as shown in Figure 3. Concentration standards of dimethyl sulfoxide (DMSO) were made by dilution in deuterated DMSO. In the DMSO dilution experiments, samples were placed in a microscope well-slide alongside a shard of glass, and fields of view were carefully composed such that the shard of glass bisected the field of view and could be used as an internal reference for leakage, Stokes spectrum, and nonresonant background. In the AXN dilution experiments the signals were sufficiently strong and clean so as to obviate this internal-standard procedure.

3. RESULTS AND DISCUSSION

3.1 Multimodal imaging of AXN using CARS and FWM

The principal result of the current study is a clear demonstration of the surprisingly large nonlinear optical response from AXN, even in its acylated form as found *in vivo*. This response, whether vibrationally resonant as in the case of CARS, or electronically resonant as in the case of degenerate-FWM, is orders of magnitude larger than any we have observed in other natural biological materials. As such, the signals are sufficiently strong as to allow for simple contrast-based, label-free imaging of AXN *in vivo*. However, commensurate with this increased optical response which allows for nonlinear optical imaging is an increased optical photosensitivity, leading to photobleaching/photodegredation at unusually low laser powers. In Figures 4(a) and (b) we show transmitted light microscope images of *H. pluvialis* cysts before and after photobleaching. In the unbleached state, the cells show a hazy mixture of green and rusty-brown regions corresponding to chlorophyll-rich and carotenoid-rich regions, respectively. It is widely believed that the synthesis of large AXN deposits is a cellular defense mechanism which prevents light-induced photo damage to chlorophyll and, thus, to the photosynthesis apparatus of the cell.[6-8] Exposure to moderately intense near-infrared laser powers leads to photobleaching of both the chlorophyll and carotenoid content. For example, exposure of the cells shown in Figure 4(a) to as little as 10 seconds of 15 mW at 915 nm nearly completely bleaches the AXN components. This can be confirmed visually by the disappearance of the rusty-brown component, as seen in Figure 4(b). Concurrent monitoring of the cells with TPEF and CARS reveals that despite visual indications that it is the carotenoid content that is predominantly bleached, in fact, both the CARS signals from AXN and the TPEF signal from chlorophyll diminish significantly over the course of a few seconds at these seemingly low fluences. An inspection of the absorption spectrum of these compounds shows no absorption features at wavelengths between 700 nm and 1100 nm, and hence we deduce that, unlike for the case of visible-light stress,[34] in our experiment photobleaching of these compounds must be due to higher-order processes.[35] In Figure 5 we present absorption spectra for both high and low concentrations of AstaReal10L, showing that AXN does not have appreciable absorbance in the Vis-NIR region for wavelengths longer than 600 nm. *In vivo* measurements of AXN-rich regions in *H. pluvialis* are identical to those obtained *in vitro* from AstaReal10L (not shown).

Despite the tendency of AXN (and chlorophyll) to photobleach at relatively low laser powers, the CARS and FWM signals are sufficiently strong to allow for sensitive very low power imaging and characterization of these components *in vivo*. Nearly background-free CARS imaging and hyperspectroscopy of AXN is enabled by utilizing any pump wavelength between 880 nm and 920 nm, with (chirped-pulse) pump powers at the sample of 3 mW. Likewise, FWM imaging of AXN is enabled by utilizing any pump wavelength between 780 nm and 850 nm, with pump powers at the sample of 1.5 mW. Under either of these conditions, strong TPEF signals enable concurrent imaging of chlorophyll-rich regions. A CARS/TPEF image of a *H. pluvialis* cell, showing contrast based on the 1520 cm^{-1} ν_1 vibrational mode in AXN is presented in Figure 4(c), and a degenerate-FWM/TPEF image is shown in Figure 4(d). These images establish that excellent contrast that can be obtained for AXN, from both CARS and FWM, depending on the pump wavelength.

Based on contrast needs alone, one might conclude that FWM imaging of carotenoids is preferable to CARS imaging. While both provide excellent contrast for AXN and enable simultaneous collection of TPEF for chlorophyll imaging, the pump wavelengths used for FWM are more readily available from commercial oscillators. In addition, the FWM experiment utilizes lower pump powers and, because is it not based on vibrational resonance imaging, the FWM signal is considerably less dependent on frequency matching conditions between the pump and "Stokes" pulses. As such, degenerate-FWM imaging of carotenoids *in vivo* is much easier to implement than CARS imaging. The spectroscopic advantages of CARS, however, are significant. Our experimental approach to CARS microscopy—one based on spectral focusing of pulses derived from a femtosecond oscillator and subsequent creation of a Stokes supercontinuum—allows for simple and rapid collection of vibrational spectra at each image pixel. Such hyperspectral

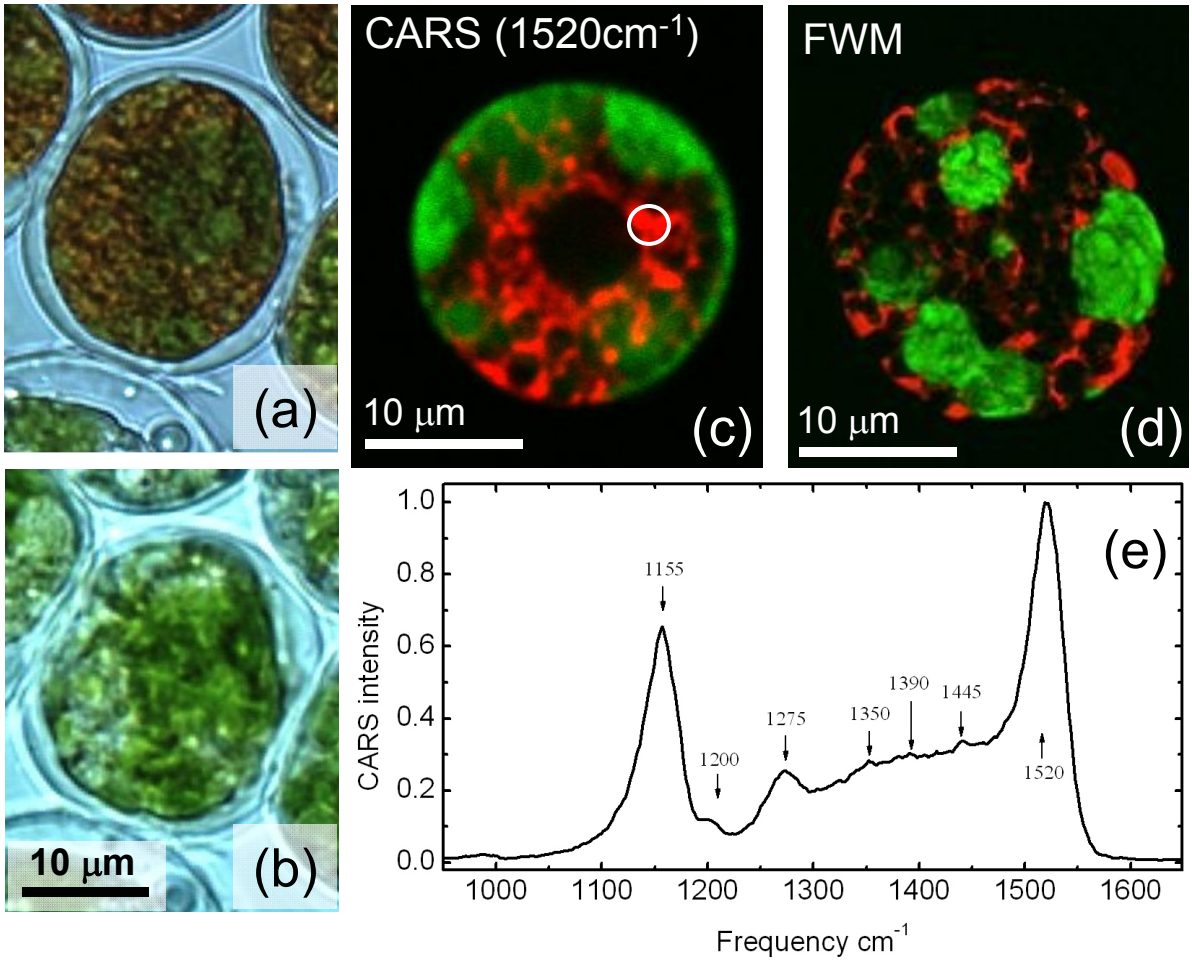

Figure 4. Label-free multimodal imaging of *H. pluvialis* cysts. (a) Transmitted light image of a typical alga cell, showing a mixture of rusty-brown carotenoid-rich regions and green chlorophyll-rich regions. (b) Transmitted light image of the same cell as in (a) after photobleaching with a one minute exposure to 15 mW of pulsed laser light. (c) TPEF (green) visualizes chlorophyll and CARS (red) visualizes AXN, showing the two cellular components to be largely segregated. 256 × 256 pixel CARS hyperspectral stacks are obtained in 5 minutes by scanning the pump-Stokes delay time. Pump wavelength was 915 nm. (d) TPEF (green) visualizes chlorophyll and FWM (red) visualizes AXN. Image is an average of five 512 × 512 images, each acquired in 1s. (e) CARS spectrum averaged over the highlighted (circled) region of interest shown in (c). Little spectral reshaping (due to nonresonant background/FWM) is observed: the CARSspectrum strongly resembles the spontaneous Raman spectrum with a spectral resolution of nom. 30 cm^{-1}. Key, known Raman peaks of AXN are identified by arrows.[36] Different fields of view are presented in (a), (c), and (d).

imaging has been shown to be extremely useful for materials characterization.[27,36-38] Furthermore, particularly in AXN-rich samples where CARS signals are so large as to dominate any NRB contamination, the CARS spectrum closely resembles the spontaneous Raman spectrum and can provide sensitive characterization of carotenoids *in vivo*. This feature seems to confirm preliminary reports of background-free CARS imaging of carotenoids in other microflora.[14] In Figure 4(e) we present the raw CARS spectrum obtained from the highlighted region of interest in the CARS image of Figure 4(c). As expected, two main vibrational resonances in carotenoids, the C-C vibration at $\nu_2 \approx 1150$ cm^{-1} and the C=C vibration at $\nu_1 = 1520$ cm^{-1}, dominate the spectrum, with weaker resonances between the two being clearly resolvable.[11,36] The relatively weak CH_3 stretching mode at $\nu_3 \approx 1008$ cm^{-1} is largely absent from the raw spectrum due to a deficiency of spectral power within Stokes supercontinuum at the requisite frequency.

3.2 Dependence of CARS signals on AXN concentration

AXN concentration *in vivo* can be very high, and therefore CARS spectra from cellular deposits are very well resolved. By comparing these signals to CARS signals from a reference sample of pure diamond (at 1335 cm^{-1}), we found that *in vivo* signals from AXN deposits can be as much as two orders of magnitude larger than from diamond obtained under identical experimental conditions. This represents an immense CARS response, one that should allow for the rapid, real-time imaging of even dilute cellular carotenoid content. The concentration dependence of the CARS signal at 1520 cm^{-1} in dilutions of AstaReal10L in canola oil confirms (i) that the quadratic dependence of CARS signal on concentration is maintained down to the lowest measureable concentrations of 1.7 mM, and (ii) that even at the lowest concentrations, resonant CARS signals dominate over the NRB. In Figure 5 we present a comparison of the CARS concentration dependence and spectral shape of AXN and DMSO. DMSO is used solely as a standard reference liquid with large, known CARS response. The DMSO dilution assay was obtained using 30 mW of pump power, wheras that from the AXN assay used 3 mW of pump power. Both used very similar power densities in the Stokes beam. From inspection of Figure 5, we can estimate that CARS signals are roughly equivalent at 0.22 M DMSO and 0.0018 M AXN. For both samples, the expected quadratic dependence of CARS signal on pump power is also observed (not shown).[18,19] Thus, we can estimate that *per molecule* CARS signals from AXN in the fingerprint region are on the order of 10^4-10^6 times stronger than those from DMSO in the CH region. Furthermore, as can be seen from Figure 5, while the NRB interferes with the CARS signal of DMSO such that considerable spectral reshaping takes place and the two vibrational resonance peaks are shifted to lower frequencies, this effect is not observed at even the lowest measurable concentrations of AXN. For example, in the background-subtracted spectrum for 1.8 mM AXN, the five identified resonances (shown as arrows in Figure 5) are commensurate with their known Raman frequencies, and are at the same spectral position as found in the spectrum from concentrated AXN *in vivo*, shown in Figure 4(e). The ability to use CARS microscopy to spectroscopically image an important cellular constituent down to (or below) 2mM is a significant result, and is among the lowest sample concentrations for which a CARS microscopy spectrum has been shown in the literature.[39,40]

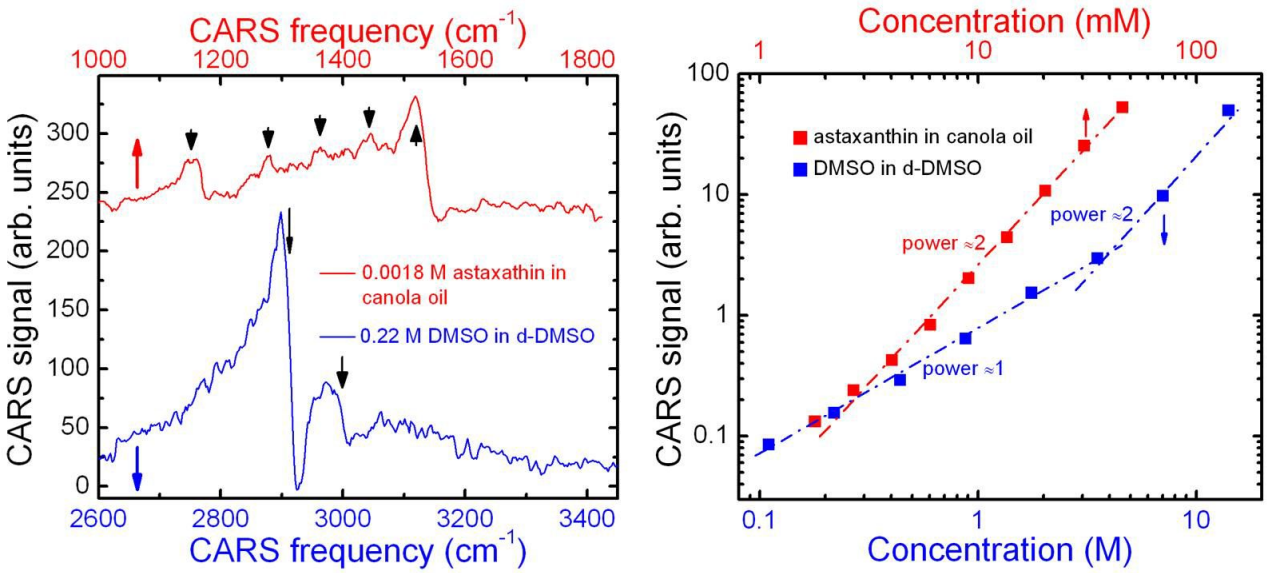

Figure 5. Concentration dependence and CARS spectra of AXN and dimethyl sulfoxide (DMSO). In both panels, the bottom axis and colour red is used for AXN data and the top axis and colour blue is for DMSO data. Left panel: background-subtracted CARS spectra from dilute samples of DMSO in deuterated DMSO and acylated AXN in canola oil. The C-H vibration region spectrum from 0.22 M DMSO and the fingerprint region spectrum from 1.8 mM AXN (shifted upwards vertically) are presented. Black arrows designate expected peak locations based on known spontaneous Raman spectra. Thus, spectral reshaping due to the NRB is considerably more pronounced in the DMSO spectrum compared to that in AXN. Right panel: A log-log plot showing concentration dependence of peak CARS signals in DMSO and AXN dilution experiments. While the CARS signal transitions from the expected power (slope) of 2 to a linear dependence at fairly high concentrations of DMSO, the lack of nonresonant background signal in the AXN sample allows for the observation of quadratic dependence down to 2 mM.

3.3 Resonance enhancements of CARS and FWM signals in AXN

Several aspects of our results lead to questions regarding the origin of the increased strength of both the CARS and FWM signals in AXN. Foremost, as described above, the magnitude of the CARS response at e.g. 1520 cm^{-1} in AXN is several orders of magnitude larger than we typically observe in other samples known for the strength of their vibrational response. For example, the fact that CARS signals from AXN-rich regions of *H. pluvialis* cells can be up to 250 times larger than the signals we obtain from bulk diamond is startling. This is especially true once we estimate that the most concentrated deposits are approximately 150-300 mM carotenoid in a lipid matrix (approx. 70% of saturation), and are thus far from being pure AXN (~1.8 M). Secondly, it is curious that the nondegenerate FWM signal is so strong when pumping with wavelengths below 850 nm, but that it is almost undetectable when pumping at wavelengths above 880 nm—where the fingerprint CARS signal dominates. We have data showing that at a pump wavelength of 860 nm, the CARS signal at 1520 cm^{-1} dominates over the FWM signal, but the latter now adds a significant NRB component to the CARS spectrum. Thus, the FWM signal shows strong wavelength dependence. With these observations in mind, the simplest explanation for the large CARS and FWM responses involves (electronic) resonance enhancement of the two processes.[24,39,41] For such an enhancement, one or more wavelengths in the CARS/FWM process should be resonant with an appropriate transition in AXN. For CARS, the pump, Stokes, and/or anti-Stokes should be resonant with a dipole-allowed transition, while for degenerate FWM, twice the frequency of the pump should be resonant with a two-photon allowed transition.[20] However, as seen from the overlay of the known energy levels of AXN with the CARS and FWM excitation scheme energies, no such resonance is observed. We can easily confirm the lack of such a (one-photon) resonance in the CARS process by noting the absence of any meaningful absorbance features in the absorption spectrum of AXN, as shown in Figure 3. In particular, it remains unclear why a turn-over is observed from a strong electronic FWM signal in AXN at pump wavelengths below 850 nm, to a very weak FWM signal at wavelengths above 880 nm. Unfortunately, with our present experimental conditions, the measurement of any significant reduction in the enhancement of the CARS signal at 1520 cm^{-1} for pump wavelengths below 860 nm is inaccessible because of unavailability of the required ($\lambda < 990$ nm) Stokes light from the PCF. The precise location of the $3A_g^-$ level is unknown and its location on the diagram in Figure 1 is estimated from the literature.[42] However, if this level is in fact at a slightly higher energy, it could be a plausible source for the requisite two-photon enhancement of the FWM observed at the lower wavelengths. If the large CARS response from AXN is due to an electronic resonant enhancement, its source is unknown at present. It is tempting to appeal to a "pre-resonance" affect,[43] but the main transition at 480 nm is at least 8000 cm^{-1} removed from the nearest relevant wavelength of the anti-Stokes pulse (at 800 nm). Strong, largely wavelength-independent, spontaneous Raman responses from carotenoids have been previously observed in the near-IR.[44] This been attributed to a π-electron/phonon coupling mechanism proposed for long polyene chains,[45] rather than to traditional resonance enhancement. It is possible that this mechanism is consistent with our CARS data, but its relevance to nonlinear optical processes is unclear. Unfortunately, neither absolute Raman intensities nor Raman intensities referenced to any standard sample have been reported in the literature for carotenoids excited with wavelengths greater than 600 nm. In our estimations, the CARS responses as a function of pump wavelength presented here are disproportionately larger than those found in spontaneous Raman experiments. We are currently investigating this relationship in greater detail. It is expected that, all things being equivalent, relative CARS signals should scale quadratically with the Raman response, thus making such comparisons between spontaneous Raman and CARS measurements of carotenoids in the near IR may provide answers regarding potential resonance enhancement effects in the CARS process. The strict quadratic dependence of the CARS signal on pump power seems to eliminate the possibility that the large signals are a result of exotic processes of higher-order than CARS/FWM. In our future investigations, we will explore the possibility that the large CARS signals from *in vivo* AXN originate in either long-lived cationic radicals,[46] or in carotenoid aggregates.[47,48] Our preliminary data, however, strongly contradicts such hypotheses.

4. SUMMARY

We have demonstrated the utility of multimodal CARS hyperspectroscopy for the *in vivo* characterization of carotenoid (and chlorophyll) content in microalgae. Extremely strong CARS signals can be obtained with considerably less pump power than we typically use for CARS imaging of any other compound. When pumping with wavelength between 880 nm and 920 nm, the strong CARS signals are devoid of nonresonant background, a fact that both increases

image contrast and precludes commonly observed reshaping of the CARS spectrum. A study of *in vitro* concentration dependence confirms that the CARS signal remains quadratic down to the lowest measured concentrations of 1.8 mM astaxanthin. Furthermore, even at the lowest concentrations the signal is sufficiently strong that low-power pumping leads to spectra that are dominated by resonant signals (as opposed to NRB) with resonances appearing unshifted from their expected spontaneous Raman frequencies. Thus, the ability to simultaneously collect strong TPEF signal from cellular chlorophyll together with an ability to monitor dilute cellular concentrations of AXN should allow for live (and non-destructive) investigations of carotenogenesis in microalgae and bacteria. Furthermore, the fact that spectral peaks are observed at their precise Raman frequencies means that AXN (or other similar carotenoids) could be used for direct spectral calibration of CARS frequencies in many experimental setups. In addition to vibrationally-resonant (CARS) imaging, we show that for more common laser excitation schemes, utilizing pump powers between 780 nm and 850 nm, the nonresonant background signal—a manifestation of electronic FWM—itself becomes so strong and dominant that it too can be used for high-contrast imaging of carotenoids *in vivo*. Unlike CARS, the FWM signal does not strongly depend on the energy difference between the pump and "Stokes" beam, and thus represents an experimentally simpler approach to contrast imaging of carotenoids. Because the excitation schemes for CARS and FWM are identical, the same experimental setup can be used for either approach, with the only significant difference being the pump laser output wavelength. The immense strength of the CARS and FWM signals suggests the existence of electronically resonant enhancement conditions, but both the absorption spectrum and analysis of the well-studied energy levels in astaxanthin seem to preclude such an effect. Thus the source of the strength of the CARS and FWM signals remains unclear.

ACKNOWLEDGMENTS

This research was funded in part by a CFI Leaders Opportunity Fund grant (at Trent University), NSERC Discovery Grants (at Ottawa and Trent Universities), and an NSERC CREATE program for Quantitative Biomedicine (at University of Ottawa). We thank Stephen O'Leary (NRC, Halifax) for support and Michael S. Schuurman and Marek Z. Zgierski (NRC, Ottawa) for helpful discussions on theoretical aspects of caratenoid Raman spectroscopy. We thank Rune Lausten, Doug Moffat and Chris Kingston of the NRC for their expert technical assistance. We thank AstaReal for providing AstaREAL-10L® samples for study.

REFERENCES

[1] Guerin, M., Huntley, M. E. and Olaizola M., "*Haematococcus* astaxanthin: applications for human health and nutrition," *Trends in Biotechnology*, 21, 210-216 (2003).

[2] Tominaga, K. Hongo, N., Karato, M. and Yamashita, E., "Cosmetic benefits of astaxanthin on humans subjects," *.Acta Biochimica Polonica*, 59, 43-47, (2012).

[3] Yuan, J.-P., Peng, J., Yin, K. and Wang, J.-H., "Potential health-promoting effects of astaxanthin: A high-value carotenoid mostly from microalgae," *Molecular Nutrition & Food Research*, 55, 150-165, (2011).

[4] Lorenz, T. R., Cysewski, G. R., "Commercial potential for Haematococcus microalgae as a natural source of astaxanthin," *Trends in Biotechnology*, 18(4), 160-167 (2000).

[5] Droop, M.R., "Conditions governing haematochrome formation and loss in the alga *Haematococcus pluvialis* Flotow," *Arch Mikrobiol*, 20S, 391-397 (1954).

[6] Goodwin, T.W. and Jamikorn, M., "Studies in carotenogenesis. 11. Carotenoid synthesis in the alga *Haematococcus pluvialis*.,"*Biochemical Journal* 57, 376-381 (1954).

[7] Boussiba, S., "Carotenogenesis in the green alga *Haematococcus pluvialis*: Cellular physiology and stress response," *Physiologia Plantarum*, 108, 111–117 (2000).

[8] Fan, L., Vonshak, A., Zarka, A. and Boussiba, S., "Does astaxanthin protect *Haematococcus* against light damage?,"*Zeitschrift für Naturforschung*. C, 53, 93-100 (1998).

[9] Grünewald, K., Hirschberg, J. and Hagen, C., "Ketocarotenoid biosynthesis outside of plastids in the unicellular green alga *Haematococcus pluvialis*," *The Journal of Biological Chemistry,* 276, 6023-6029 (2011).

[10] Wayama, M., Ota, S., Matsuura, H., Nango, N., Hirata, A. and Kawano, S., "Three-Dimensional Ultrastructural Study of Oil and Astaxanthin Accumulation during Encystment in the Green Alga *Haematococcus pluvialis*," *PLOS One,* 8, e53618 (2013).

[11] Kaczor, A., Turnau, K. and Baranska, M., "*In situ* Raman imaging of astaxanthin in a single microalgal cell," *The Analyst*, 136, 1109-1112 (2011).

[12] Pilát, Z., Bernatová, S., Ježek, J., Šerý, M., Samek, O., Zemánek, P., Nedbal, L. and Trtílek, M., "Raman microspectroscopy of algal lipid bodies: beta-carotene quantification,"*Journal of Applied Phycology*, 24, 541-546 (2012).

[13] Collins, A. M., Jones, H. D. T., Han, D., Hu, Q., Beechem, T. E. and Timlin, J. A., "Carotenoid Distribution in Living Cells of *Haematococcus pluvialis (Chlorophyceae*),"*PLOS One*, 6, e24302 (2011).

[14] Dementjev, A. and Kostkevičiene, J., "Applying the method of Coherent Anti-stokes Raman microscopy for imaging of carotenoids in microalgae and cyanobacteria," *J. Raman Spectrosc.* 44, 973–979. (2013).

[15] Denk, W., Strickler, J. and Webb, W. "Two-photon laser scanning fluorescence microscopy," *Science* 248, 73–76 (1990).

[16] Cisek, R., Spencer, L., Prent, N., Zigmantas, D., Espie, G. and Barzda, V., "Optical microscopy in photosynthesis," *Photosynthesis Research* 102(2), 111-141 (2009).

[17] Broess, K., Borst, J. W. and Amerongen H., "two-photon excitation fluorescence lifetime imaging microscopy to study photosynthesis in plant leaves," *Photosynthesis Research*, 2009, Volume 100(2), 89-96 (2009).

[18] Volkmer, A., "Vibrational imaging and microspectroscopies based on coherent anti-Stokes Raman scattering microscopy," J. Phys. D., 38, R59–R81 (2005).

[19] Evans, C. L. and Xie, X. S., "Coherent anti-Stokes Raman scattering microscopy: chemical imaging for biology and medicine," *Annu. Rev. Anal. Chem*. 1, 883–909 (2008).

[20] Wang, Y., Lin, C.-Y., Nikolaenko, A., Raghunathan, V. and Potma, E. O., "Four-wave mixing microscopy of nanostructures," *Advances in Optics and Photonics*, 3, 1-52 (2011).

[21] Brocious, J. and Potma, E. O., "Lighting up micro-structured materials with four-wave mixing microscopy," *Materials Today* 16, 344-350 (2013).

[22] Huang, L. and Cheng, J.-X., "Nonlinear Optical Microscopy of Single Nanostructures," *Annual Review of Materials Research*, 43, 213-236, (2013).

[23] Mahou, P., Olivier, N., Labroille, G, Duloquin, L., Sintes, J.-M., Peyriéras, N., Legouis, R., Débarre, D. and Beaurepaire, E., "Combined third-harmonic generation and four-wave mixing microscopy of tissues and embryos," *Biomedical Optics Express*, 2, 2837-2849 (2011).

[24] Tolles, W. M., Nibler, J. W., McDonald, J. R. and Harvey, A., B., "A Review of the Theory and Application of Coherent Anti-Stokes Raman Spectroscopy (CARS)," *Applied Spectroscopy*, 31, 253-271 (1977).

[25] Zumbusch, A., Holtom, G. R. and Xie, X. S., "Three-dimensional vibrational imaging by coherent anti-stokes raman scattering," *Physical Review Letters,* 82, 4142-4145 (1999).

[26] E. O. Potma and X. S. Xie, "Cars Microscopy for Biology and Medicine," *Optics and Photonics News*, 15, 40-45 (2004).

[27] Pegoraro, A. F., Slepkov, A. D., Ridsdale, A., Moffatt, D. J. and Stolow, A., "Hyperspectral multimodal CARS microscopy in the fingerprint region," *J. Biophoton.*, 7, 49–58 (2014).

[28] Pegoraro, A. F., Ridsdale, A., Moffatt, D., J., Jia, Y., Pezacki, J. P. and Stolow, A., "Optimally chirped multimodal CARS microscopy based on a single Ti:sapphire oscillator," *Optics Express*, 17, 2984-2996 (2009).

[29] Hellerer, T., Enejder, A. M. K. and Zumbusch, A., "Spectral focusing: High spectral resolution spectroscopy with broad-bandwidth laser pulses," *Applied Physics Letters*, 85, 25-27 (2004).

[30] Slepkov, A. D., Ridsdale, A., Wan, H.-N., Wang, M.-H., Pegoraro, A. F., Moffatt, D. J., Pezacki, J. P., Kao, F.-J. and Stolow, A., "Forward-collected simultaneous fluorescence lifetime imaging and coherent anti-Stokes Raman scattering microscopy," *J. Biomed. Opt.* 16(2), 021103 (2011).

[31] Lyn, R. K., Kennedy, D. C, Sagan, S. M., Blais, D. R., Rouleau, Y., Pegoraro, A. F, Xie, X. S., Stolow, A, Pezacki, J. P. "Direct imaging of the disruption replication complexes of the hepatitis C virus by inhibitors of lipid metabolism" *Virology* 394, 130–142 (2009).

[32] Ko, A. C.-T., Mostaço-Guidolin, L. B., Ridsdale, A., Pegoraro, A. F., Smith, M. S. D., Slepkov, A. D., Hewko, M. D., Kohlenberg, E. K., Schattka, B., Stolow, A, Sowa, M. G., "Using multimodal femtosecond CARS imaging to determine plaque burden in luminal atherosclerosis," *Proc. SPIE* 7903, 790318 (2011).

[33] Slepkov, A. D., Ridsdale, A., Pegoraro, A. F., Moffatt, D. J. and Stolow, A., "Multimodal CARS microscopy of structured carbohydrate biopolymers," *Biomed. Opt. Express* 1, 1347-1357 (2010).

[34] Andreeva, A., Abarova, S., Stoitchkova, K., Picorel, R. and Velitchkova, M. "Selective Photobleaching of Chlorophylls and Carotenoids in Photosystem I Particles under High-Light Treatment," *Photochemistry and Photobiology*, 83, 1301–1307 (2007).

[35] Walla, P. J., Yom, J., Krueger, B. P. and Flemming, G. R., "Two-Photon Excitation Spectrum of Light-Harvesting Complex II and Fluorescence Upconversion after One- and Two-Photon Excitation of the Carotenoids," *The Journal of Physical Chemistry B*, 104, 4799-4806 (2000).

[36] Schulz, H., Baranska, M. and Baranski, R. "Potential of NIR-FT-Raman spectroscopy in natural carotenoid analysis," *Biopolymers*, 77, 212–221 (2005).

[37] Hartshorn, C. M., Lee, Y. J., Camp, C. H., Liu, Z., Heddleston, J., Canfield, N., Rhodes, T. A., Hight Walker, A. R., Marsac, P. J., Cicerone, M. T., " Multicomponent Chemical Imaging of Pharmaceutical Solid Dosage Forms with Broadband CARS Microscopy," *Anal. Chem.*, 85, 8102– 8111 (2013).

[38] Lin, C.-Y., Suhalim, J. L., Nien, C. L., Miljkovic, M. D., Diem,´M., Jester, J. V., Potma, E. O., "Picosecond spectral coherent anti-Stokes Raman scattering imaging with principal component analysis of meibomian glands.," *J. Biomed. Opt.* 16, 021104-1−021104-9 (2011).

[39] Min, W., Lu, S., Holtom, G. R., Xie, X. S., "Triple-Resonance Coherent Anti-Stokes Raman Scattering Microspectroscopy," *ChemPhysChem*, 10, 344-347 (2009).

[40] Mueller M., Schins, J. M. and Wurpel, G. W. H., "Shot-noise limited detection sensitivity in multiplex CARS microscopy," *Proc. SPIE* 5323, Multiphoton Microscopy in the Biomedical Sciences IV, 195 (2004).

[41] Dutta, P. K., Dallinger, R. and Spiro, T. G., "Resonance CARS (coherent anti‐Stokes Raman scattering) line shapes via Frank‐Condon scattering: Cytochrome c and β‐carotene," *J. Chem. Phys.* 73, 3580-3585 (1980).

[42] Polívka, T. and Sundström, V., "Dark excited states of carotenoids: Consensus and controversy," *Chemical Physics Letters*, 477, 1-11 (2009).

[43] Boas, D. A., Pitris, C. and Ramanujam, N., [Handbook of Biomedical Optics], CRC press, 246 (2011).

[44] Parker, S. F., Tavender, S. M, Dixon, N. M., Herman, H., Williams, K. P. J. and Maddams, W. F., "Raman Spectrum of beta-Carotene Using Laser Lines from Green (514.5 nm) to Near-Infrared (1064 nm): Implications for the Characterization of Conjugated Polyenes," *Appl. Spectrosc*. 53, 86-91 (1999).

[45] Castiglioni, C., Del Zoppo, M. and Zerbi, G., "Vibrational Raman spectroscopy of polyconjugated organic oligomers and polymers,"*Journal of Raman Spectroscopy*, 24, 485-494 (1993).

[46] Amarie, S., Förster, U., Gildenhoff, N., Dreuw, A., Wachtveitl, J. "Excited state dynamics of the astaxanthin radical cation," *Chem. Phys*., 373 64 (2010).

[47] Wang, C., Tauber, M. J., "High-Yield Singlet Fission in a Zeaxanthin Aggregate Observed by Picosecond Resonance Raman Spectroscopy," *J. Am. Chem. Soc.* 132, 13988– 13991 (2010).

[48] Wang, C., Berg, C. J., Hsu, C.-C., Merrill, B. A. and Tauber, M. J., "Characterization of Carotenoid Aggregates by Steady-State Optical Spectroscopy," *The Journal of Physical Chemistry B* 116 (35), 10617-10630 (2012).